Amijeet Thakur
17MF10004

Surface Roughness of Additive Manufactured parts

29th May 2020

Introduction

Three Dimensional Printing or 3D printing is a solid freeform fabrication process which creates parts directly from a computer model(generally a CAD model) by depositing in layers. Each layer is created by depositing powder and selectively joining the powder with binder applied by a modulated ink-jet printhead. Additive manufacturing (AM) [1] techniques garner much interest within many fields, such as aerospace, automotive, and medical, based on their flexibility given to designers to fabricate complex structures, which are hard to fabricate using conventional methods. By achieving lightweight structures that do not require molding and tooling, AM also saves time, cost, and effort. Also, AM plays an important role in hybrid manufacturing and smart factories [2], and it is likely a key technology in the implementation of the new industrial revolution, the Industry 4.0. [3]

AM has a multi-disciplinary characteristic and its standardization is essential for the industrial sector. The main organizations which are working and collaborating to standardize the processes of AM are the International Organization for Standardization, the technical committee ISO/TC 261 (creation date 2011), the American Society for Testing and Materials, the group ASTM F42 (formed in 2009), and the European Committee for Standardization, the technical committee CEN/TC 438 (formed in 2015). ISO/ASTM 52900-15 established and defined terms used in AM technology, by defining AM as the “process of joining materials to make parts from three-dimensional (3D) model data,

usually layer upon layer, as opposed to subtractive manufacturing and formative manufacturing methodologies" [4]. Based on the ISO/ASTM 52900-15 standard, the AM processes are classified as follows [4]:

1. Vat photo-polymerization (VP)
2. Binder jetting (BJ)
3. Material extrusion (ME)
4. Material jetting (MJ)
5. Sheet lamination (SL)
6. Powder bed fusion (PBF)
7. Directed energy deposition (DED)

Some examples of the technologies that fall within these processes types include stereolithography (SLA) as a VP process [5], fused deposition modeling (FDM) as an ME process [6], laminated object manufacturing (LOM) as an SL process [7], selective laser sintering/melting (SLS/SLM) as a PBF processes [8,9], 3D inkjet printing (3DP) as a BJ process [7], polymer jetting (PolyJet) and multi-jet printing (MJM) as MJ processes [10–12], wire and arc additive manufacturing (WAAM) and laser-engineered net shaping (LENS) as DED processes [13]. The performance characterization of the AM processes and material characterization are significant tasks for their standardization and implementation in the industry. A method for evaluating AM process performance consists of manufacturing and testing a customized sample [14]. The most important sections, focusing on test methods and product characterization of the parts manufactured by AM [4], are mechanical properties (hardness, tensile strength, flexural strength, impact strength, fatigue strength, elongation property, compressive properties, creep, aging, frictional coefficient, shear resistant, crack extension), surface aspects (appearance, surface texture [15], color), and geometry requirements [16] (size, dimensions, dimensional tolerances, geometrical tolerance). Currently, the standards related to these items are under development. A number of experimental and theoretical studies were developed in order to characterize the variety of AM processes and the materials used for AM.

Some barriers to adoption of 3D - Printing

1. Cost:

The capital cost of industrial-grade 3D printers is still quite large therefore capital cost is proving to be a major barrier for many SMEs (small and medium enterprises), who cannot afford such high capital costs. But what customers usually are not aware of is the even higher running costs. Therefore users and potential customers demand more cost transparency over which machine they should buy and what will be the total capital and the running cost to keep printing what they want. This is one limitation of 3D printing for industrial applications that could and should be resolved sooner rather than later.[17]

2. Materials:

The materials issue continues to be a limitation for design engineers and manufacturing engineers when it comes to 3D printing for prototyping applications. As the name suggests 3D - Printing or rapid prototyping is usually used to quickly make prototypes directly from the Computer Aided Design model. This is generally used to test certain important physical properties of the designed part. Therefore testing functionality of new products is a key application for 3D printing, one that could grow exponentially if engineering grade materials were available more readily. Typical 3D printing materials such as ABS and PLA suffer from being quite weak, which limits their usefulness for functional prototyping. In reality, applications have to be carefully selected to suit the materials, when surely it should be the other way around.[17]

3. Input required: 3D Data:

The fuel for 3D printing is a design of the item that is to be printed. And that fuel must be created in three dimensions — whether from scratch in design software like CAD or from 3D scanning techniques to capture the geometry of an already existing part. This can be a contentious issue with industrial users tending to get

quite vocal about 3D design software. There are many sites where these discussions can be viewed to assess current issues, which include costs (high), features (or lack thereof), interoperability (low), ease of use (it isn't) and 'printability,' to name a few. Easy input is essential for mainstream industrial adoption of 3D printing. Most customers complain about CAD models and available software not being fully ready or user friendly enough for printing most 3D models out there. For 3D printing to revolutionise the manufacturing industry features like Integrated scanning, measuring, part analyzing and part recording should all be within the capability of a 3D printer unit.[17]

4. Full colour capabilities:

Some industrial designers are quite dismissive of the need for 3D printing color capabilities in the design and prototyping process. Some believe 3D printers should focus on accuracy and precision and pretty colors are not of high importance to the manufacturing industry. For most, however, it is the catalyst for this technology sector in creating aesthetically realistic prototypes and fully manufactured parts that require little or no finishing. After a few colour capable machines being launched in the market, people have now seen the potential of color, and as more and more have realized the benefits of it, it has become something many 3D printing users now want, expect or demand.[17]

5. Accuracy & Surface Finish:

Most of the users complain accuracy and surface finish as being major issues. The problem is that high accuracy is possible with some of the 3D printing processes, which quite legitimately boast extremely fine, impressive tolerances, but the parts that these processes produce are extremely fragile and next to useless for functional testing. When strength and robustness are built into the parts, surface finish is sacrificed and requires specific skills and many man-hours to finish the part to acceptable levels. Until this particular trade-off is resolved, the applications for 3D printing will remain relatively limited, and alternative tools for getting the job done — more quickly and efficiently — will always win out. Why wouldn't they?

This is not to denigrate where 3D printing works — when it works it is spectacular— but for greater adoption, this is a fundamental issue that still needs to be addressed.[17]

Reasons for high surface roughness on the Additive manufactured parts

3D printing, also known as additive manufacturing or rapid prototyping is a manufacturing technique by which metal parts can be 'printed' using a variety of materials including metals directly by using it's CAD(Computer Aided Model) model. Direct fabrication of functional end-use parts can be manufactured by a variety of methods for example, SLS (Selective Laser Sintering) and melting of metal powders by means of laser irradiation. Even with today's extensive research, experimental trials, and computational prediction, all process parameters cannot be optimised to obtain a 3D printed part with a surface finish at-par with a machined one. Although there are many reasons why a part being 3D printed can have poor surface quality, the few main reasons are:

1. The first one being because of the very nature of how 3D printing works. This reason for poor surface quality can only be made negligible and can never be completely removed. This is mainly because the Computer Aided Design (CAD) model of the part being printed is preliminarily sliced into thin layers, the resulting contour of the real part is a stepped approximation of the nominal surface. This is known as the staircase effect. It has been proved that a staircase effect is induced depending on both the local theoretical curvature and the sloping angle with the building direction. Although the thickness of the building layers can theoretically be reduced to improve surface finish, obviously the thickness cannot be made infinitesimally thin since there is a threshold of minimum slicing which depends upon the average powder grain size of the material used. A distinct lay pattern (i.e., a distinct directional feature) is hence produced on the surface, depending on the building direction. This poor surface quality can be reduced by methods like

post-processing and machining. Figure 1 shown below demonstrates the unavoidable staircase effect in 3D printing.[18]

FIGURE 1

2. The second reason is how the part orientation is while being printed. To demonstrate how important this reason is, let us take a real example. Consider a cylinder with a hole (10 mm outer diameter, 6 mm inner diameter, 30 mm length) that is printed with FDM with its center axis vertical. The 3D printer would construct this part as a series of concentric circles layered on top of one another. This would produce a final cylinder with a relatively smooth outer surface. If the same cylinder is reorientated with its center axis horizontally, the part will be built as a series of rectangles (with slightly different width) layered on top of each other. Also, the surface of the cylinder that touches the build platform will be flat, because the material would as the initial first layers were printed. By orienting the part in different directions, there is a significant difference in the print quality, this can be observed in figure 2. The cylinder in the right was printed laterally and the one on the left was printed axially. Here the difference in surface quality and defect in base quality can be easily seen by eye-inspection. [18]

FIGURE 2

3. As 3D printed parts are built layer by layer, a previous layer to build upon is required. With FDM printing, each layer is printed as a set of heated filament threads which adhere to the threads below and around it. Each thread is printed slightly offset from its previous layer. This allows a model to be built up to angles of 45°, allowing prints to expand beyond its previous layer's width. When a feature is printed with an overhang beyond 45°, it can sag and requires support material beneath it to hold it up, as demonstrated in figure 3.[18]

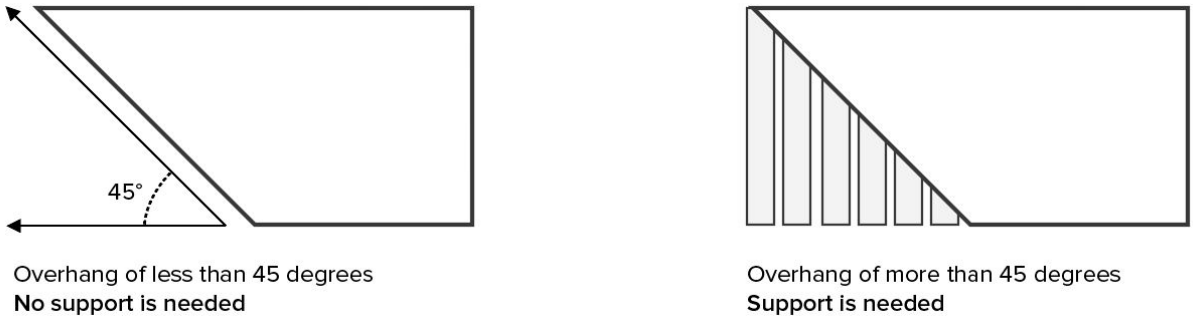

FIGURE 3

The ABCs (or YHTs) of FDM support: Consider the letters Y, H, and T, and a set of associated 3D models (figure 4). The arms of a model of the letter Y can be printed easily. Even though the arms of the Y are outstretched, because they extend at 45 degrees or less, they do not require support. The letter H is a little more complicated but if the center bridge is under 5mm, it can be printed without support or any sagging. Over 5mm and support will be required. For this example, the center bridge is over 5mm and support is needed. The letter T requires support for the arms of the letter. There is nothing for the outer arms to be printed on and the material will just fall down without support.

Therefore depending on the specific 3D Printing technology and the complexity of the 3D model, this can mean that a 3D print requires support structures. When considering what technology to print a 3D model with, it is important to consider support structures and how they may affect the final result. Hence support structures will have an impact on surface finish as they require post-processing

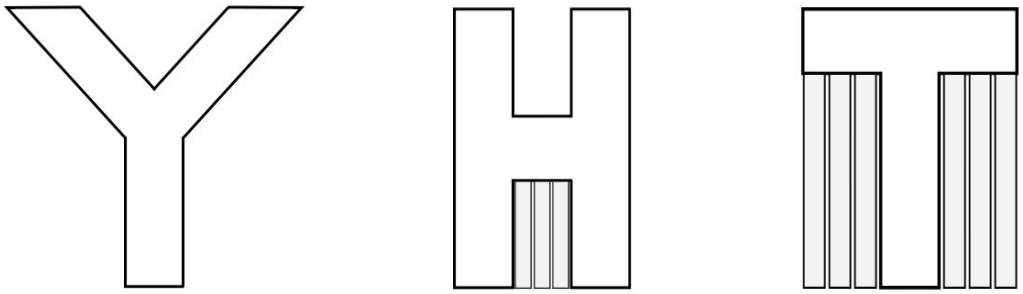

FIGURE 4

work to remove them, resulting in blemishes and surface roughness. Therefore supports will always need post processing like grinding and laser treatment to obtain the required surface quality. [18]

Hence, depending on the technology and the average powder grain size—standards for surface finish may not be evenly matched on a single complex part. Depending on the manufacturer, the powder size, build orientation and the need for support for overhangs and the layer thickness, arithmetic as-built roughness usually ranges from 8 to 20 microns, whereas tighter standards could be required. Also Therefore, post processing for the purpose of surface modification in terms of morphology and roughness is required. Several methods can be considered for post processing like computer numerical control (CNC) machining, shot peening, sandblasting, infiltrating, grinding, etc.

Issues or problems due to high roughness

There are various issues related to high surface roughness. Since surface finish quality of 3D printed parts is becoming more and more vital with more 3D printed parts being directly used for end-user purposes. Surface finish quality is critical not only for an appealing aesthete but also for a better functionality of the part being printed. For example, if a gear is 3D printed, the surface roughness of those surfaces which mate with the next gear has to be smooth for proper functioning of the gear system. The gear system could face problems like greater machine noise, low power transmission, reduced machine life and several other complications and unwanted outcomes. Hence in

addition to material properties like tensile strength, ductility, hardness, fatigue strength, creep strength, etc, surface quality is also a very important property of the part being 3D printed.

Even though 3D printing has the advantages of being an additive manufacturing process in a market where most manufacturing processes are reductive in nature, the extra machining costs required to increase the surface quality usually negates the less material being used in 3D printing. Moreover a good surface finish will also save a ton of post-processing time required to improve the surface quality of the 3D printed part by machining. Therefore a good surface finish is desired by every manufacturer or researcher using rapid prototyping in their manufacturing or prototyping needs.

Strategies or methods used to reduce surface roughness during additive manufacturing.

As we all know, decreasing the layer thickness while manufacturing would certainly improve the surface quality of the part, but this is not always the most ideal thing to do as decreasing the thickness of each layer would drastically increase the time taken to print the part. Also there is a threshold minimum to which one can reduce the surface roughness of the part being 3D-printed, where even better surface quality is required. There are a few ways by which we can improve the surface quality of the 3D printed part without compromising with the time taken to print it or without reducing the layer thickness of each layer.

Process parameters of additive manufacturing processes and machine advancements to reduce surface roughness.

1. Adaptive slicing:

In literature a wide variety of approaches has addressed the problem of analyzing [19,20] and improving surface roughness of rapid prototyped parts. This last category can be roughly subdivided into four categories, namely (i) optimal build direction, (ii) slicing strategy (iii) fabrication parameters optimization, (iv) post-treatment. Categories (i)

and (ii) address the reduction of roughness due to the staircase effect, while (iii) and (iv) include more general approaches that can also be applied to surfaces not affected by the staircase effect, such as horizontal surfaces. To optimize the building direction (i) some examples are reported in ref. [21]. To reduce roughness the authors establish decision criteria and develop algorithms based on the considerations of surface quality, building time, and the complexity of support structure, as a means of identifying desirable fabrication orientations for a given design.

FDM technology has been investigated in ref. [22] where two aspects are considered: roughness and manufacturing time optimization. These opposite issues are both improved by using an adaptive slicing scheme. Models for evaluating the average part surface roughness and building time have been developed. A coded genetic algorithm is used to obtain the optimal solution. In ref. [23] a more recent study is reported, that focused on optimal construction direction finding for different rapid prototyping techniques, using a multi-criterion decision method. The importance of part orientation and build direction is stressed, as it affects the product roughness, manufacturing building time and cost. To minimize the required post-machining region (RPMR) in the product, an intelligent methodology for determining the optimal fabrication direction is proposed. An equation expressing the distribution of surface roughness is presented and the relation between the RPMR and the fabrication direction is investigated, taking real layered manufacturing environments into consideration. Then, a genetic algorithm is applied to obtain a reliable solution for a complex geometry CAD model. To improve slicing strategies (ii), the most widely investigated approach is adaptive slicing. In adaptive slicing, the number of layers are drastically reduced by using sloping layer walls. For vertical and sloping outer walls, the strategies for determining slice height generally take into account a number of vertical sections along the contour of a slice. Surface deviation error is calculated at these sections and then slice height is determined. In traditional adaptive slicing the user imposes a single surface finish requirement for the whole object. In literature, region-based adaptive slicing has been proposed [24] where the user is free to impose different surface finish requirements on different surfaces of the model. In ref. [25] a method is proposed to compute the error over the surface. This

method approximates the outer wall between two successive contours by a series of taut cubic spline patches. The deviation between the patch and the actual surface is considered to yield a better and more exhaustive estimate of surface error. The predicted number of slices is slightly higher than the number predicted by existing methods for sloping layer walls. An example of category (iii) is reported in [26], where roughness and dimensional errors are evaluated. A benchmark with several dimensional, geometrical, and surface roughness features is used and the Taguchi experimental design method is developed to find the least number of experimental runs and best process parameter settings. Several measurements are performed while evaluating the stereolithography part quality to find the functional relationships between the output part quality and the input manufacturing process parameters. In ref. [27] a slicing method ensuring unilateral tolerance over the whole prototype is proposed. The slicing rule is chosen by computing the inner product of the part's normal vector on an STL file and the working direction, together with the desired function of the part to be manufactured. The error is reduced by adopting proper solutions proposed for geometric shapes that lose their qualities easily, such as peaks, valleys, flat areas and fine features. The amounts of tolerance volume and effective cusp are computed to facilitate post-processing of the part and slicing procedures are proposed and experimentally verified. Finally, for category (iv), in ref. [28] the reduction of surface roughness is approached by using CNC milling machines, focusing on the development of the CNC program, once the part has been produced by layer deposition. Unfortunately, when complex surfaces with small details have to be realized this approach is time-costly because of the layered fabrication, the machining setup, the generation of the CNC code and the subtractive machining phase. Moreover, complex features remain inaccessible. In literature [29] abrasive flow machining (AFM) has been experimented also for the manufacture of holes or small complex shaped surfaces but this is limited by poor precision of the viscous agent pressure distribution, that can lead to non-homogeneous material removal from the workpiece. In ref. [30] abrasive jet deburring is used to improve the surface roughness of rapid prototypes. The processing parameters such as flow pressure and time are firstly studied, then dimensional errors and roughness reductions are measured.

In ref. [31] a semi-empirical model for the evaluation of the surface roughness of a layered part manufactured by fused deposition modeling is presented. The surface finish of FDM rapid prototyped components is improved by using a simple material removal method consisting of hot cutter machining (HCM). The drawback is that certain areas of the prototyped component remain inaccessible. Very recently Stratasys, the owner of the FDM patent, has launched in the market a semi-automated finishing system for ABS parts [32,33]. However, it is very costly, the operator is heavily involved in the evaluation of the surface finish, and post-curing time is long (12–18 h).

2. Optimal Scanning Technique:

Also new research aiming to improve surface quality of Rapid Prototyped parts has led to some new findings. Almost all previous research on optimal build orientation refers to the orientation of the object as a whole. It is argued that as the layer thickness is getting thinner with the ever developing RP technologies, the orientation of the object is no longer the major factor affecting part surface quality, instead it is found that the scanning orientation on layers that influence more on part surface quality. Therefore choosing an optimal scanning technique would greatly improve our surface quality apart from decreasing the layer thickness and choosing an optimal build direction. [34]

3. Various smoothing techniques:

There is another smoothing method to reduce the stepping effect on SL rapid prototyped parts. This method is accomplished by following procedure: after a layer is drawn by laser beam, the part is lifted up to a single layer thickness, and scanned by the laser according to the concave corner between the horizontal and vertical extended edges of the lifted layer. The incidence angle of the laser beam affects the solidification profiles of the SL resin. This technique is used to smooth the surface roughness of the SL parts. The roughness value was somewhat improved by generating an inclined solidification profile according to the longitudinal direction of the line connection which connects the two convex points of a stair step on each layer. However, no improvement was found for surface roughness on surfaces of 40° or less from horizontal because of the laser refraction characteristics of the SL resin. While this kind of research uses

in-process techniques to improve the surface roughness of RP parts to some degree, several problems remain. Namely, improvement to the domain of the surface is limited by building material property. Consequently, total processing time is longer due to re-coating and hardening. [35]

Various metal 3D printing and their typical resolutions are: [36]

Metal AM Process	Resolution in microns µ
PBF(Powder Bed Fusion)	20-200
Powder DED(Directed Energy Deposition)	100-1,000
Joule Printing	500-1,000
Wire DED(Directed Energy Deposition)	2,000-50,000

Processes used for finishing of Additive manufactured parts. What is the minimum surface roughness achieved by the finishing process on the Additive manufactured parts ?

1. **Shape Additive Grinding**

   This process was applied to post processing of titanium alloy (Ti6Al4V) additively manufactured by EBM(Electron beam melting) and SLS(Selective laser sintering). The shape adaptive grinding (SAG) process expands upon the processed bonnet concept whereby an inflated and tilted spherical membrane tool is used to machine a surface. This bonnet tool is normally covered with a polishing cloth, and a stream of abrasive slurry is directed at the tool and recirculated. As the bonnet presses against the surface of the workpiece (controlled by the tool-offset), the contact-spot diameter increases.

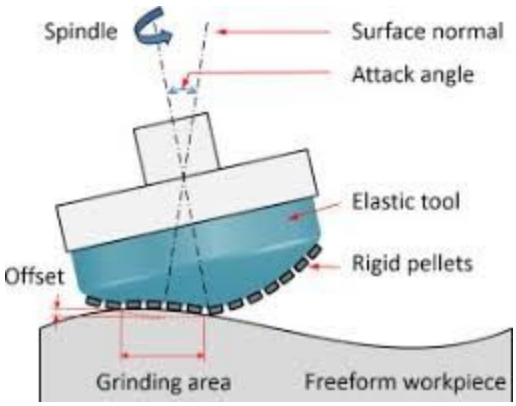

FIGURE 5

But in the SAG process, instead of being covered with a polishing cloth the rubber bonnet (elastic tool) is covered with nickel bonded (NBD) or resin bonded (RBD) diamond pellets.. The deformability of the elastic layer allows the tool to conform to freeform surfaces featuring any convex curvature, or concave curvature larger than about twice the radius of the spherical SAG tool. However, at a smaller scale the diamond pellets act as a rigid tool and allow for grinding to take place. The result is a shape adaptive grinding process with the benefits of both polishing and grinding techniques. This allows for greater material removal than standard polishing techniques, while achieving low surface roughness on complex freeform shapes.

The spindle speed, attack angle, tool offset, and surface speed of the tool can be actively controlled by a 7-axis CNC machine as it traverses the surface of the workpiece. This allows for control of the grinding spot in terms of contact area and removal rate. The air pressure inside the bonnet can also be varied in order to control the grinding force according to the hardness of the metal or the desired surface roughness . Finally, water is typically used as a coolant.

Experimental procedure: Flat Ti6Al4V samples produced by EBM and SLS were procured for the basic grinding experiments. The typical condition of the EBM manufactured surfaces is shown in Figure 6, as measured by a confocal laser microscope. The surface roughness ranged between 4 and 5 µm Ra. A series of

experiments were conducted to determine the range of surface roughness and removal rate achievable with the SAG tools.

For the surface roughness experiments, a series of 5 x 45 mm sub-sections of the titanium sample were ground using the machining parameters shown in Table 1: The work spindle was operated at 75% of the maximum speed (1500 rpm) for optimal productivity combined with limited thermal expansion of the spindle, (i.e. frictions in the mechanical bearings). Tool pressure of 1.0 bar, attack angle of 20°, and tool offset of 0.3 mm were selected in accordance with previous experience of the SAG process [37]

. The tool feed rate was allowed to vary across the subsections, with step values of 25, 50, 100, 200, and 400 mm/min. For each sub-section, the optimal feed for which the rate of improvement in surface roughness tailed off was recorded. From one sub-section to the next, the nominal size of final diamond abrasives in the SAG pellets was decreased from 40µm down to 3µm, until a smooth surface could be obtained.

For the removal rate experiments, another sample of titanium was ground using the machining parameters shown in Table 2: The work spindle was operated at 75% of the maximum speed (1500 rpm), the tool pressure was set to 1.0 bar, attack angle 20°, and tool offset 0.3 mm, which were selected in accordance with previous experience of the SAG process. The tool feed rate was kept constant in these experiments, and after each grinding pass the removal rate was characterized by generating influence spots (dwelling of the tool at a static location).

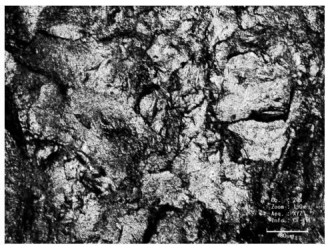

FIGURE 6. Laser microscope image (20x) of Ti6Al4V sample produced by EBM.

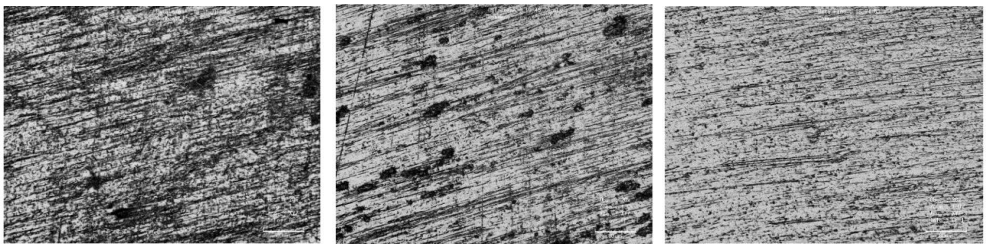

a. Nickel bonded 40 µm c. Nickel bonded 9 µm e. Resin bonded 3 µm

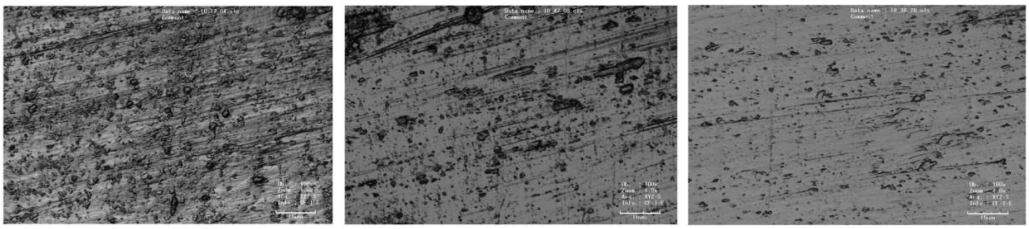

b. Nickel bonded 40 µm d. Nickel bonded 9 µm f. Resin bonded 3 µm

FIGURE 7

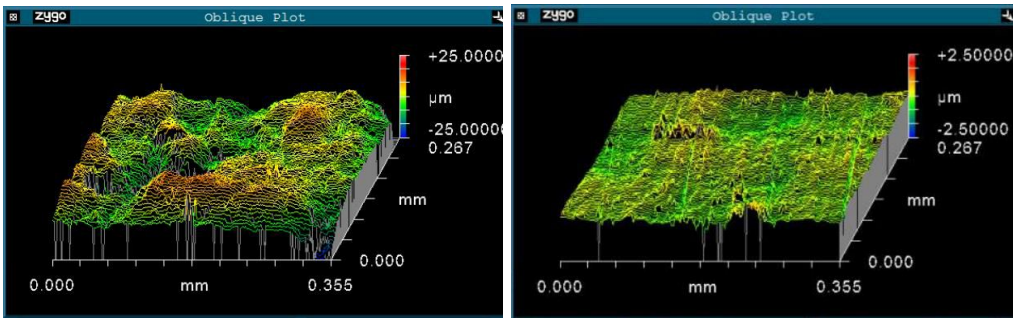

a. As received b. Nickel bonded 40 µm

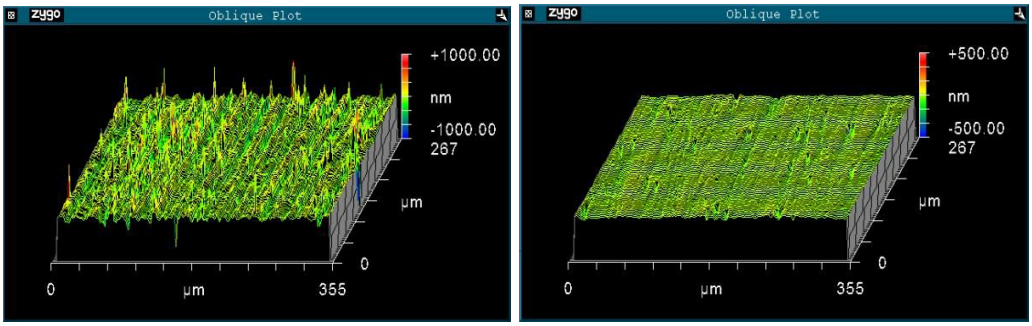

c. Nickel bonded 9 µm d. Resin bonded 3 µm

FIGURE 8

Table 1

Parameter	Value
Workpiece	
Shape	Flat
Material	Ti6Al4V
Process	EBM and SLS
Machine parameters	
Attack angle	20°
Spindle speed	1500 rpm
Tool pressure	1.0 bar
Tool offset	0.3 mm
Raster spacing	0.3 mm
Surface feed (Roughness experiment)	25, 50, 100, 200, and 400 mm/min
Surface feed (Removal experiment)	50 and 100 mm/min
Grinding Tools	
Tool radius	10 mm
Abrasive size	40, 9 and 3 µm
Abrasive type	Diamonds bonded in nickel and resin pellets

Table 2

Parameter	Value
Workpiece	
Shape	Freeform
Material	Ti6Al4V
Process	SLS
Machine parameters	
Attack angle	20°
Spindle speed	750 rpm
Tool pressure	1.0 bar
Tool offset	0.2 mm
Raster spacing	0.21, 0.20, 0.19 mm
Surface feed (Roughness experiment)	200 mm/min
Grinding Tools	
Tool radius	10 mm
Abrasive size	40, 9 and 3 µm
Abrasive type	Diamonds bonded in nickel and resin pellets

Surface roughness: Figure 7 shows laser microscope images of the surface at 20x and 100x magnification, after reaching optimal surface roughness on the EBM samples with each SAG tool (progression on the SLS samples was similar). Figure 8 shows three-dimensional profiles of the same areas taken with a white light interferometer at 10x magnification.

Due to the rough initial condition of the surface, shown in Figure 6 and 7(a), a coarse 40 µm nickel bonded diamond (NBD) SAG tool was initially used to remove the

micro-structured surface layer. Figure 8(a), 8(b) shows the resulting surface, in which the structured layer was mostly removed, allowing for finer grinding with subsequent SAG tools.

After pre-grinding of the next subsection at optimal feed rate with the 40 µm NBD tool, a 9 µm NBD tool was used. Further reduction in the surface microstructures was observed as shown in Figure 8(c), 8(d) and 8(c). But the emergence of a directional surface texturing (aligned with the grinding direction) could also be observed.

The next subsection was prepared by passes with the 40 µm and 9 µm NBD tools at optimal feed. The tool used for final smoothing was the 3 µm resin bonded diamond (RBD) SAG tool. The grinding direction was aligned perpendicular to that of the previous 9 µm NBD tool. The final surface shows attenuation of the directional scratches, and low surface roughness below 10 nm Ra, as seen in Figure 8(a), 8(b) and 8(c). These results show substantial improvement by more than one order of magnitude when compared with other methods for post-processing additively manufactured titanium.

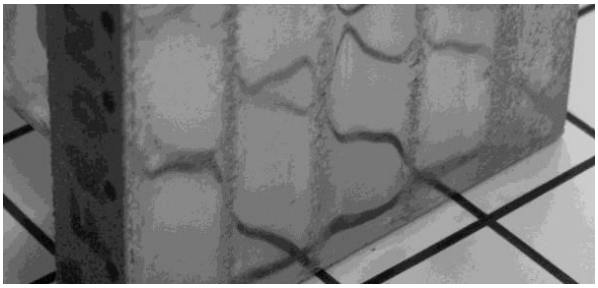

FIGURE 9

A photograph of the ground EBM sample is shown in Figure 9. This picture shows the surface condition at various successive grinding stages from right to left: after 40 µm grinding, after 40 µm + 9 µm grinding, and after 40 µm + 9 µm + 3 µm grinding (the left edge of the workpiece shows the original surface condition). It can be seen that the surface progressively became more reflective after each successive grinding run.

Figure 10 shows the evolution of surface roughness Ra at 10x magnification on the EBM (blue) and SLS (red) samples with successive SAG tools, as a function of grinding time

across the 5 x 45 mm sub-sections. On each spline regression curve, the markers indicate the progressive decrease of feed rate from 400, 200, 100, 50, down to 25 mm/min.

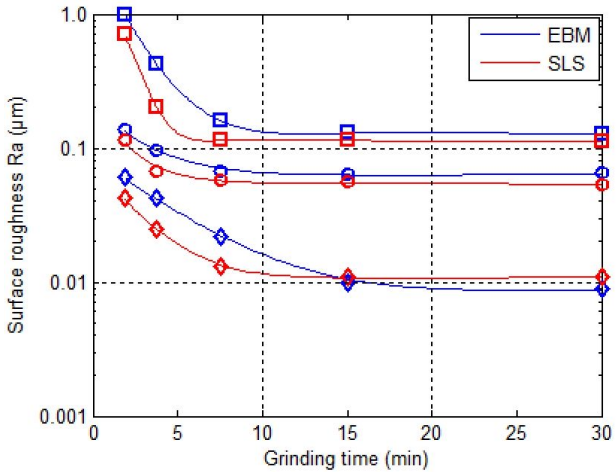

FIGURE 10 Evolution of surface roughness Ra on EBM (red) and SLS (blue) samples, as a function of grinding time for each SAG tool.

Based on this evolution of roughness versus feed rate, it was found that optimal grinding could be obtained by using the following steps:

1. EBM: 100 mm/min with 40 µm and 9 µm nickel bonded diamond SAG tools, and 50 mm/min with 3 µm resin bonded diamond SAG tool.
2. SLS: 200 mm/min with 40 µm and 9 µm nickel bonded diamond SAG tools, and 150 mm/min with 3 µm resin bonded diamond SAG tool.

For 5 x 45 mm sub-sections, these conditions equated to 30 minutes total grinding on EBM, and 15 minutes total grinding time on SLS.

Removal rate: Characterization of the removal rate is an important factor determining the extent to which the SAG process can be used to finish artifacts without significant degradation of their original dimensional accuracy. For this reason, the various SAG tools were used to grind a workpiece for 60 minutes each, and the removal rate was determined every 30 minutes by dwelling a few seconds at static locations to generate influence spots. The spot depth was then measured with a profilometer, and used to

compute the equivalent volumetric removal rate, as shown in Figure 11 (the observed removal rates were consistent between EBM and SLS samples, and are plotted here with linear regressions).

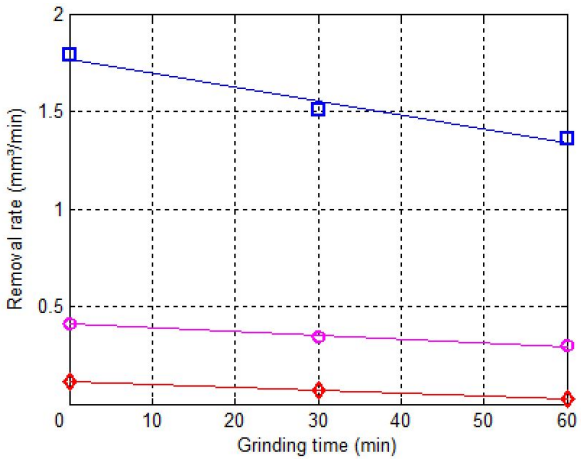

FIGURE 11. Evolution of removal rate as a function of grinding time for each SAG tool.

The set of 10 mm radius SAG tools spanned a range of volumetric removal rates of approximately 1 order of magnitude, from about 0.1 mm3/min for the resin bonded 3 µm diamonds up-to 2 mm3/min for the nickel bonded 40 µm diamonds. It was also found that the removal rate could be scaled up by increasing the radius of the SAG tools, or through usage of the CNC controller variables such as higher spindle rotation, or increased attack angle.

The removal rate of the SAG tools was found to follow a linear decline over time, which was consistent from tool to tool. In order to keep the depth of removal approximately constant during grinding passes, the most practical solution depends on the size of the artifact to be ground: in the case of small surfaces, grinding with multiple quick passes shorter than 20 minutes each, rather than a single slower pass, is adequate. In the case of larger surfaces, it is possible to mitigate the issue by programming in the tool path software an inverse compensation of the decline into either surface feed or spindle rotation, and thus maintain better consistency of the absolute depth of removal.

Applications to freeforms

Experimental procedure: The application of the SAG process to freeform shapes was demonstrated on a complex sample prepared by state-of-the-art SLS. Figure 12(a) shows a photograph of the additively manufactured workpiece as received. The surface condition was superior to that of the flat EBM sample. Figure 12(b) shows a rendering of the corresponding CAD model, with the area to be finished in blue. It can be noticed that this shape includes convex, concave, and saddle areas. The surface curvature ranged from 30 mm radius (concave) to 10 mm radius (convex).

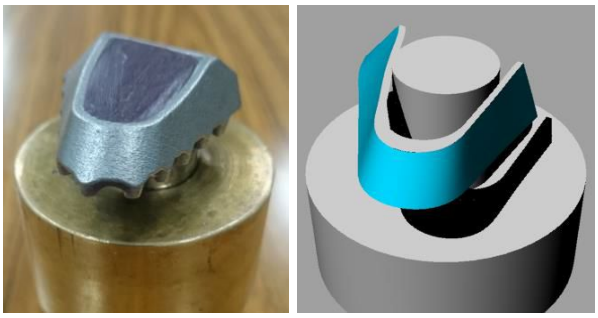

a)As received b) Area to be ground (blue)

FIGURE 12. Freeform sample prepared by SLS.

A 7-axis CNC controlled machine built by Zeeko ltd was used for grinding this freeform sample. The SAG tools were mounted such that the center of the machine A and B rotary axes coincided with the center of the spherical tool, as shown in Fig. 13.

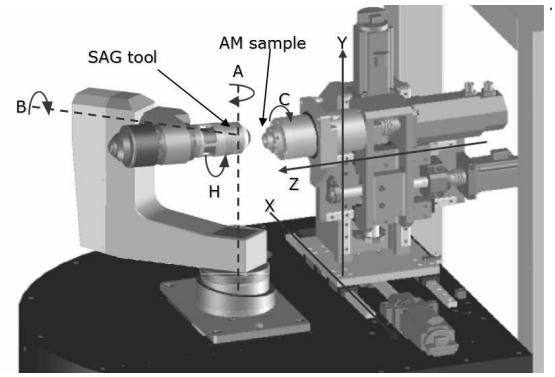

FIGURE 13. 7-axis freeform machining center.

This mounting allows for motion of the grinding spot around the workpiece with high precision of the tool offset (which controls the grinding area), because the spherical tool remains static (varying only its orientation) while the workpiece is accurately translated along the X, Y, and Z axes.

In order to characterize and compensate the deviation between CAD model and actual workpiece, an on-machine probing system was used. A soft probe was mounted on the tool spindle, and used to detect the surface by touch/trigger sensing mode. The machine software was programmed to probe a 3D array of points as shown in Fig. 14(a). The resulting data was then freeform fitted to the CAD model to determine the workpiece location inside the machine, and the residual form deviation against the CAD model. This data was used to compensate for the CNC tool path.

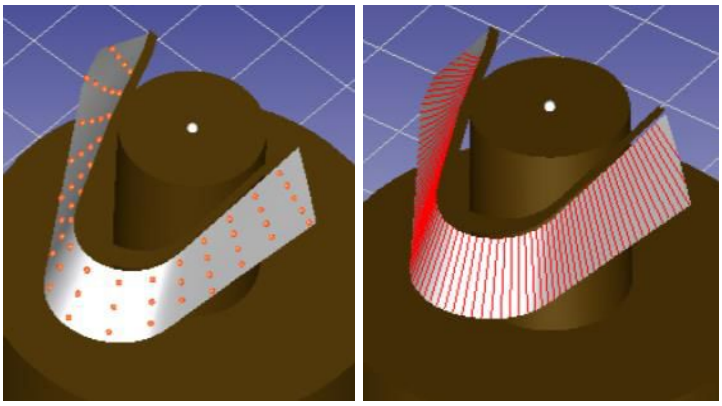

a) Grid of probe point b) Tracks of raster path

FIGURE 14. Definition of the probing and tool path in the CAD/CAM software.

Since the 3D volumetric errors of the CNC machine had not been fully calibrated, this method could not be used to provide absolute measurements of the freeform shape. Nevertheless, prior to the grinding experiments the probing repeatability was ascertained to be better than 0.5 µm rms. Consequently, relative changes in the form error could be tracked between grinding runs by subtracting before and after measurements, which provided an estimate of the 3D removal function with an accuracy better than 0.5 µm rms.

In order to produce a raster path, the freeform shape was sectioned with a series of planes scanning along the length of the surface to be ground, as shown in Figure 14(b). 3 SAG passes were performed with mostly identical tool path parameters, as shown in Table 2. Only the raster track spacing was reduced from run-to-run, in order to prevent a build-up of raster tracks.

The other process parameters were chosen to produce a tool path within the dynamic range of the machine. They also reflected the faster processing condition of SLS material compared to EBM. The total grinding time was thus 45 minutes, consisting of 14 min with nickel bonded 40 µm, 15 min with nickel bonded 9 µm, and 16 min with resin bonded 3 µm.

The other process parameters were chosen to produce a tool path within the dynamic range of the machine. They also reflected the faster processing condition of SLS material compared to EBM. The total grinding time was thus 45 minutes, consisting of 14 min with nickel bonded 40 µm, 15 min with nickel bonded 9 µm, and 16 min with resin bonded 3 µm.

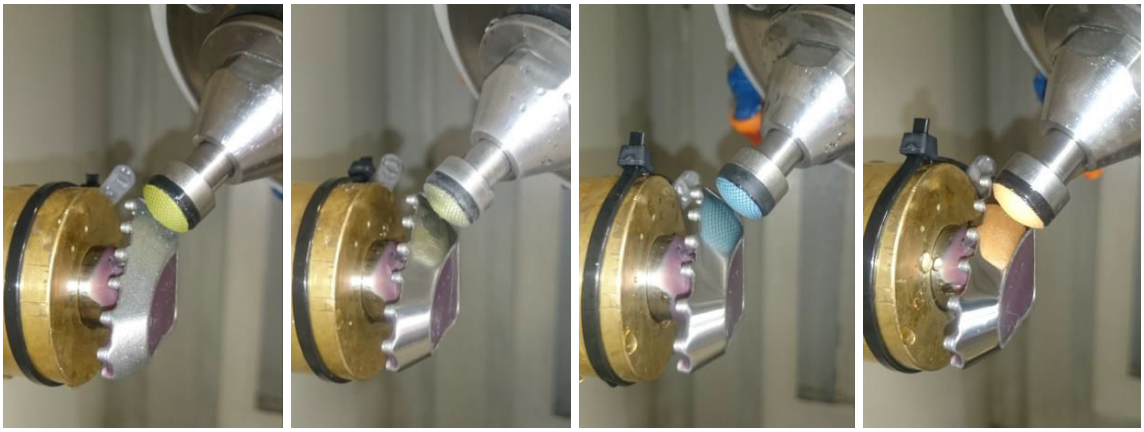

(a) As received (b) Nickel bonded 40 µm (c) Nickel bonded 9 µm (d) Resin bonded 3 µm

FIGURE 15. Condition of freeform sample after successive grinding runs.

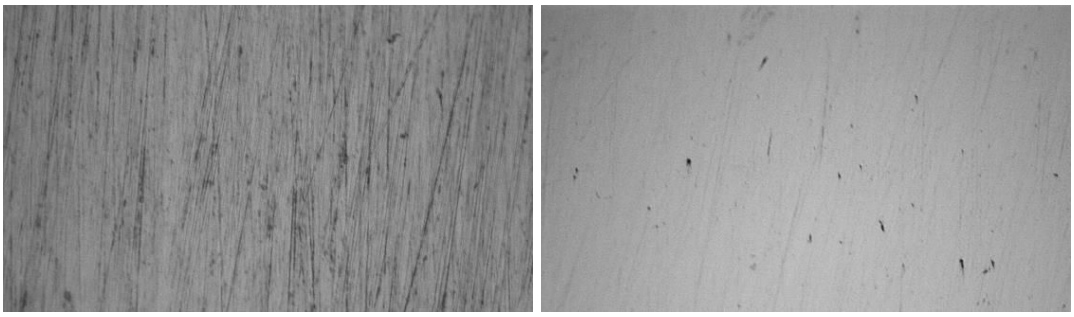

(a) After grinding with resin bonded 3 µm (b) After final polishing with 1 µm diamond paste

FIGURE 16. Optical microscope images of freeform surface taken at 100x magnification.

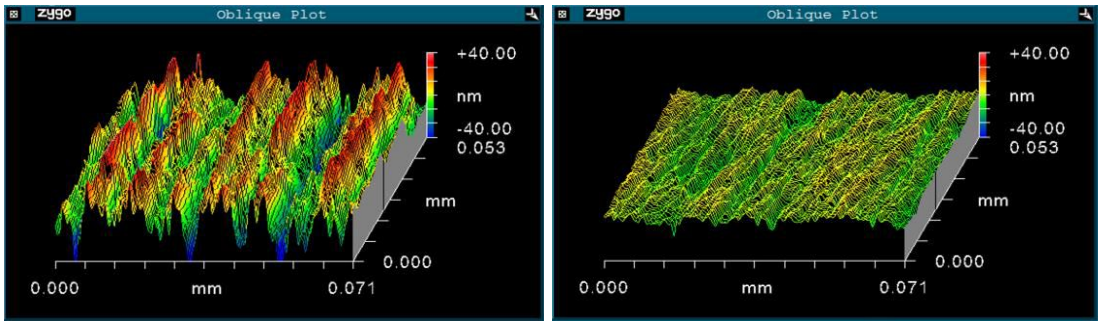

(a) After grinding with resin bonded 3 µm (b) After final polishing with 1 µm diamond paste

FIGURE 17. 3D measurements of freeform surface taken at 100x magnification.

Surface Roughness: Starting from the original AM surface condition (with roughness above 5 µm Ra), it was possible to achieve a mirror-like surface after only 3 SAG grinding runs. Figure 15 shows photographs of the surface after each grinding step from (a) to (d). The progressive improvement in surface reflectivity can be easily observed in these photographs.

After the third grinding run by resin bonded 3 µm diamonds, the surface was measured with both optical microscope and whitelight interferometer at 100x magnification (the lower 20x magnification was not practical, due to the wide variations in surface curvature). Figure 16(a) and 17(a) show the resulting surface topography. The residual grinding marks and surface roughness of 12.8 nm Ra observed after grinding on the freeform surface were very similar to those observed on the flat sample prepared by SLS. It can also be noted that substrates produced by state-of-the-art SLS technology

delivered finishing with fewer residual pores than EBM, which would indicate a superior melting condition.

In order to further improve the surface condition, a final smoothing run was performed using the same machine with a bonnet type polishing tool of similar shape and dimension as the SAG tools. A felt polishing cloth was employed together with 1 µm diamond paste. The polishing tool path parameters were slightly different than the grinding parameters: spindle speed of 400 rpm, attack angle 10, and track spacing 0.18 mm were selected, based on previous experience with diamond polishing [38]. After this final 17 min polishing run, the surface was measured again as shown in Fig. 16(b) and 17(b). The grinding marks were mostly removed, leaving a very smooth surface with roughness below 3 nm Ra.

Dimensional Accuracy: The freeform sample was probed on-machine between grinding runs using the touch/trigger probe described earlier. Figure 18(a) shows an example of probing points scattered around the fitted theoretical CAD shape of the freeform sample. The residual error was computed by projecting the points along surface normals, and recording the length of the projection vectors. Figure 18(b) shows the residual error of the sample as received, and 18(c) the residual error after the 3 steps grinding (a low-pass filter with 5 mm cut-off was applied to remove spikes). It can be seen that the overall magnitude and distribution of the peaks and valleys remained similar before and after SAG grinding.

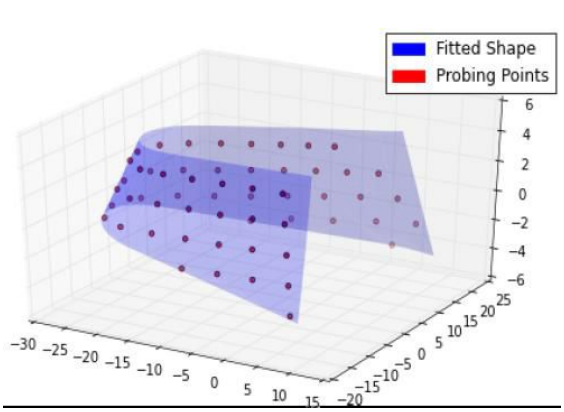

(a) Probing points and fitted CAD shape

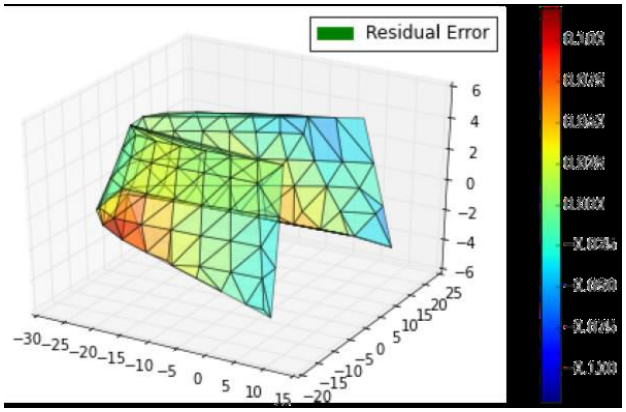

(b) Residual error (as received)

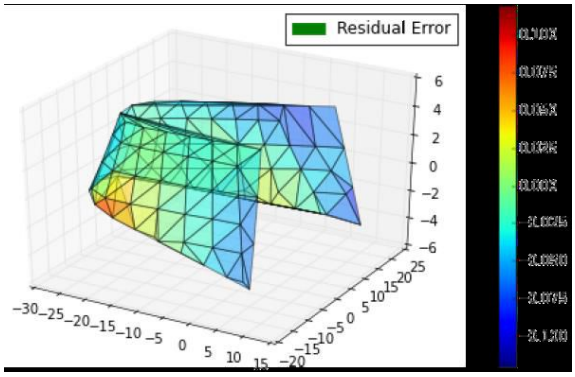

(c) Residual error (after SAG grinding)

FIGURE 18. Probing data and residual errors

In theory, the volumetric removal should have amounted to the combination of: 14 min at 0.895 mm3/min (nickel bonded 40µm), 15 min at 0.138 mm3/min (nickel bonded 9µm), and finally 16 min at 0.038 mm3/min (resin bonded 3µm). Taking into account the total surface area of 639 mm2, the average removal depth on the ground surface was thus expected to be 23.8 µm. The actual removal depth was estimated by subtracting the residuals errors shown in Fig. 18. The resulting estimation of the material removal map is shown in Fig. 19. The actual average removal depth of 25.6 µm agreed with the target within 10%, with an overall deviation of +/- 3.5 µm.

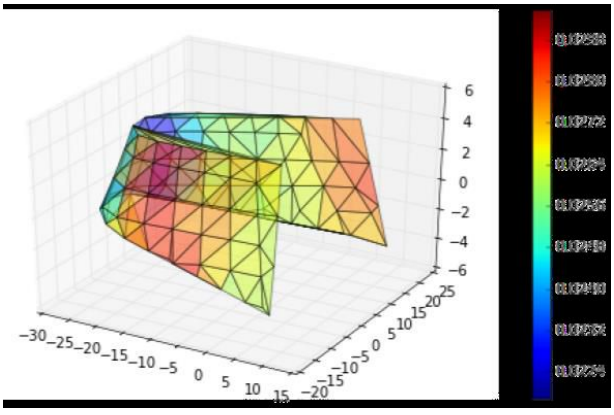

FIGURE 19. Actual material removal map.

In this material removal map, the area with lowest removal corresponds to the front of the workpiece where curvature is most convex, whereas the areas of highest removal

correspond to the sides where curvature is most concave. This result can be explained with the relative increase in grinding area that occurs when transitioning from convex to concave areas if the same tool offset is applied.

When compared to the typical accuracy of additively manufactured metal samples, usually ranging from dozens to hundreds of microns [39], the form degradation that occurred during SAG finishing is acceptable for most current applications, whether medical or aeronautics. Nevertheless, the ability of using SAG finishing in a deterministic way, that is to improve the dimensional accuracy of additively manufactured artifacts, would surely open new frontiers in precision engineering of rapidly prototyped components. For this reason, improvements in the control software will be investigated in the future so as to produce a predictive model of the removal rate as a function of surface curvature. The aim will be to achieve uniform removal across surfaces with wide curvature changes in the first instance, and corrective finishing from a known shape deviation in the second instance.

2. **Laser Post-processing**

   When finishing is driven by a laser beam, laser surface modification (LSM) is in place: namely, surface peaks are melted to fill the valleys, resulting in a smoother surface, provided that overmelting is prevented [40]. Depending on the laser operation mode, two processes are reported [41]: macro-polishing with continuous wave emission and micropolishing with pulsed radiation. As a consequence of tight focusing, laser energy is effectively delivered where required, thus suitably affecting the surface and preventing uncontrolled thermal penetration, distortion of the base metal, and thermal stresses leading to possible cracking and fatigue failure; furthermore, non-contact processing and automation are allowed. Nevertheless, the laser beam in heat treating is partially reflected, thus the absorbed energy and the eventual response depend on the surface type [42]. Hence, for the starting surface texture: the higher the starting roughness, the lower the reflectivity, and the intensity distribution and pulse duration are also involved[43] in metals.

It has been shown [44,40,13] that the main parameter in macro polishing is energy density Es depending on delivered power P, focus diameter D, and processing speed s:

$$Es = P \setminus D.s \qquad (1)$$

An energy density on the order of 30 J/mm2 has been proven to be effective[40] in reducing the roughness by at least 80% over metal sintered parts of bronze-infiltrated stainless steel[44]; similar values have been considered in optimizing post-processing on 316 L stainless steel. On the same subject, the possibility of laser polishing within the building machine and upon removal of surrounding non-melted powder has been investigated[45] using an energy density ranging from 1 to 10 J/mm2, resulting in a reduction of 70% at most on 316 L stainless steel. Alternation between manufacturing and polishing has been proposed[46] to address non-accessible surfaces in the building machine. Nevertheless, laser polishing in the same machine is deemed to be easily feasible as a final step of building when manufacturing is conducted by means of powder injection (i.e., laser metal deposition) instead of powder bed [47].

It is worth noting that LSM by means of scanning optics can be performed effectively. Galvanometers moving laser-grade mirrors with low mass and inertia are arranged to deflect the laser beam in two dimensions [48] so as to conveniently position the focus on the work-piece, although joined mechanical and optical positioning and focus adjustment are required over 3D parts. To provide uniform irradiance and scanning rate across the focal plane, an F-theta lens must be considered; with respect to standard flat-field scanning lenses, the need for complex electronic correction of the scanning speed is prevented. Higher speed, optimised exposure strategies, and larger working distances are allowed, in addition to general advantages of laser material processing with robot moved laser heads, accuracy and capability to address complex 3D geometries are benefits. Given these reasons, processing via scanning optics is a subject of

considerable interest both in research and industry to perform laser cutting, engraving, marking and surface finishing[49].

For testing An EOSINT M270 commercial laser sintering system (EOS, Krailling, Germany) has been used to manufacture a suitable number of testing samples, 3 mm thick. Pre-alloyed, argon gas atomized virgin commercial EOS GP1 stainless steel powder, 20µm mean grain size, corresponding to standard UNS S1740 chromium-copper precipitation hardening steel in terms of nominal chemical composition has been considered.

Surface modification by means of laser beam is effective as a possible post processing treatment over stainless steel components resulting from additive manufacturing, in order to improve the surface topography. The response has been proven to depend on the starting features of the samples; namely, major improvements are achieved over 45°- and upright-built samples, the process being capable of reducing arithmetic roughness below 2 µm on average, thus matching the requirement for real parts in valid operating conditions. A less significant reduction to 5 µm has been shown in the literature [50], hence 70% with respect to initial roughness can be achieved within each single trace on stainless steel additive manufactured surfaces. Moreover, the results refer to polishing upon removal of non-melted powder within the building chamber, with consequent issues to accessing a general 3D part. Additionally, reduced spot sizes are allowed when polishing in the building machine, thus multiple passes would be required over a large surface.

A valuable reduction of roughness to 1.4µm (on the order of 80%) has been achieved over stainless steel parts by using a custom-made hybrid re-cladding machine for a given processing speed ranging from 0.4µm to 0.6 m\min [44]**.** Here, it has been shown that an increased speed of 2m\min-- resulting in reduced processing processing time for a given surface extension--is possible. Even higher speeds on the order of 3m\min are reported in the literature [51], although up to 5 overlapped passes are required to properly smooth the surface below 1 µm.

Nevertheless, since a change in the microstructure is induced as a consequence of laser processing, the effects on the parent metal must be addressed. Specific benefits are offered when performing laser beam wobbling compared with linear scanning: heat effects are proven to be lower, based on the depth of the fusion zone as well as on the extent of the HAZ resulting from Vickers microhardness testing. For given operating power of 1 kW and processing speed of 2 m·min−1, wobbling with 2 mm amplitude at 200 Hz frequency is suggested. With respect to the laser path, an oscillating beam had been proposed previously in the literature [52], resulting in a reduction of roughness up to 92% over AlSi10Mg additive manufactured parts, but a one-dimensional scanning system was used.

Interestingly, additional opportunities are offered, as the resulting features of the surfaces can be conveniently graded by means of proper setting of frequency and amplitude, with reliable monitoring from the laser source. For these reasons, grounds for application on real parts are given, although additional studies on overlapping traces must be conducted to perform the process over larger surfaces.

Minimum surface roughness achieved : 0.01µm - 0.1µm

References

1. Gibson, I.; Rosen, D.W.; Stucker, B. Additive Manufacturing Technologies; Springer-Verlag: New York, NY, USA, 2015.
2. Chu, W.S.; Kim, M.S.; Jang, K.H.; Song, J.H.; Rodrigue, H.; Chun, D.M.; Cho, Y.T.; Ko, S.H.; Cho, K.J.; Cha, S.W.; et al. From design for manufacturing (DFM) to manufacturing for design (MFD) via hybrid manufacturing and smart factory: A review and perspective of paradigm shift. Int. J. Precis. Eng. Manuf. Green Tech. 2016, 3, 209–222. [CrossRef]
3. Kang, H.S.; Lee, J.Y.; Choi, S.; Kim, H.; Park, J.H.; Son, J.Y.; Kim, B.H.; Noh, S.D. Smart manufacturing: Past research, present findings, and future directions. Int. J. Precis. Eng. Manuf. Green Tech. 2016, 3, 111–128. [CrossRef]
4. International Organization for Standardization. Standard Terminology for Additive Manufacturing—General Principles—Terminology; ISO/ASTM 52900-15; International Organization for Standardization: Geneva, Switzerland, 2015.
5. Campbell, R.I.; Martorelli, M.; Lee, H.S. Surface roughness visualization for rapid prototyping models. Comput. Aided Des. Appl. 2002, 34, 717–725. [CrossRef]
6. Perez, M.; Medina-Sánchez, G.; García-Collado, A.; Gupta, M.; Carou, D. Surface quality enhancement of fused deposition modeling (FDM) printed samples based on the selection of critical printing parameters. Materials 2018, 11, 1382. [CrossRef] [PubMed]
7. Byun, H.S.; Kwan, H.L. Determination of the optimal build direction for different rapid prototyping processes using multi-criterion decision making. Robot. Comput. Integr. Manuf. 2006, 22, 69–80. [CrossRef]
8. Strano, G.; Hao, L.; Everson, R.M.; Evans, K.E. Surface roughness analysis, modelling and prediction in selective laser melting. J. Mater. Process. Technol. 2013, 213, 589–597. [CrossRef]
9. DebRoy, T.; Wei, H.L.; Zuback, J.S.; Mukherjee, T.; Elmer, J.W.; Milewski, J.O.; Beese, A.M.; Wilson-Heid, A.; Ded, A.; Zhang, W. Additive manufacturing of metallic components—Process, structure and properties. Prog. Mater. Sci. 2018, 92, 112–224. [CrossRef]
10. Chen, Y.; Lu, J. RP Part Surface quality versus build orientation: When the layers are getting thinner. Int. J. Adv. Manuf. Technol. 2013, 67, 377–385. [CrossRef]
11. Cazon, A.; Morer, P.; Matey, L. PolyJet technology for product prototyping: Tensile strength and surface roughness properties. Proc. IMechE Part B J. Eng. Manuf. 2014, 228, 1664–1675. [CrossRef]
12. Kumar, K.; Kumar, G.S. An experimental and theoretical investigation of surface roughness of poly-jet printed parts. Virtual Phys. Prototyp. 2015, 10, 23–34. [CrossRef]

13. Bandari, Y.K.; Williams, S.W.; Ding, J.; Martina, F. Additive manufacture of large structures: Robotic or CNC systems? In Proceedings of the 26th International Solid Freeform Fabrication Symposium, Austin, TX, USA, 12–14 August 2015; pp. 17–25.
14. Moylan, S. Progress toward standardized additive manufacturing test artifacts. In Proceedings of the ASPE 2015 Spring Topical Meeting Achieving Precision Tolerances in Additive Manufacturing, Raleigh, NC, USA, 26–29 April 2015; pp. 100–105.
15. Leach, R. Metrology for additive manufacturing. Meas. Control 2016, 49, 132–135. [CrossRef]
16. Umaras, E.; Tsuzuki, M.S.G. Additive manufacturing-considerations on geometric accuracy and factors of influence. IFAC-PapersOnLine 2017, 50, 14940–14945. [CrossRef]
17. https://www.engineering.com/3DPrinting/3DPrintingArticles/ArticleID/4666/3D-Printing-Barriers-to-Adoption-Part-1.aspx
18. https://www.3dhubs.com/knowledge-base/supports-3d-printing-technology-overview/
19. Ippolito R, Iuliano L, Gatto A (1995) Benchmarking of Rapid Prototyping Techniques in Terms of Dimensional Accuracy and Surface Finish. Annals of the CIRP 44(1):157–160.
20. Armillotta A (2006) Assessment of Surface Quality on Textured FDM Prototypes. Rapid Prototyping Journal 12(1):35–41.
21. Lan P, Chou S, Chent L, Gemmilt D (1997) Determining Fabrication Orientations for Rapid Prototyping with Stereolithography Apparatus. Computer Aided Design 29(1):53–62.
22. Thrimurthulu K, Pandey P, Reddy N (2004) Optimum Part Deposition Orientation in Fused Deposition Modelling. International Journal of Machine Tools & Manufacture 44:585–594.
23. Ahn DK, Kim HC, Lee SH (2007) Fabrication Direction Optimization to Minimize Post-Machining in Layered Manufacturing. International Journal of Machine Tools and Manufacture 47(3–4):593–606.
24. Mani Ka, Kulkarni Pa, Dutta Da (1999) Region-Based Adaptive Slicing. Computer-Aided Design 31(5):317–333.
25. Kumar M, Choudhury AR (2002) Adaptive Slicing with Cubic Patch Approximation. Rapid Prototyping Journal 8(4):224–232.
26. Zhou J, Herscovici D, Chen C (2000) Parametric Process Optimization to Improve the Accuracy of Rapid Prototyping Stereolithography Parts. International Journal of Machine Tools & Manufacture 40:363–379.
27. Chiu YY, Liao YS, Lee SC (2004) Slicing Strategies to Obtain Accuracy of Feature Relation in Rapidly Prototyped Parts. International Journal of Machine Tools & Manufacture 44:797–806.
28. Kulkarni P, Dutta D (2000) On the Integration of Layered Manufacturing and Material Removal Process. International Journal of Machine Science and Engineering 122:100–108.
29. Williams RE, Melton VL (1998) Abrasive Flow Finishing of Stereolithography Prototypes. Rapid Prototyping Journal 4:56–67.

30. Leong KF, Chua CK, Chua GS, Tan CH (1998) Abrasive Jet Deburring of Jewellery Models Built by Stereolithography Apparatus. Journal of Materials Processing Technology' 83:36–47.
31. Pandey PM, Reddy NV, Sanjay. Dhande G (2003) Improvement of Surface Finish by Staircase Machining in Fused Deposition Modelling. Journal of Material Processing Technology 132:323–331.
32. http://www.stratasys.com/uploadedFiles/North_America/Products/Smoothing_Station/Stratasys_FinishingStations.pdf
33. Espalin D, Medina F, Wicker R (2009) Vapor Smoothing, A Method for Improving FDM-Manufactured Part Surface Finish, Int. Rep. of the W.M. Keck Center for 3D Innovation, Univ. of Texas at El Paso, provided by Mrs. C. Gerling, Fortus Marketing Association, Stratasys Inc.
34. Yonghua Chen & Jianan Lu. "RP part surface quality versus build orientation: when the layers are getting thinner." Int J Adv Manuf Technol (2013) 67:377–385.
35. Daekeon Ahn, Hochan Kim, Seokhee Lee. "Fabrication direction optimization to minimize post-machining in layered manufacturing." D. Ahn et al. / International Journal of Machine Tools & Manufacture 47 (2007) 593–606.
36. https://www.digitalalloys.com/blog/surface-roughness/
37. Beaucamp A, Namba Y, Combrinck H, Charlton P, Freeman R. Shape adaptive grinding of CVD silicon carbide, Annals of the CIRP. 2014; 63(1): 317-320.
38. Beaucamp A., Namba Y., Inasaki I., Combrinck H., Freeman R. Finishing of optical moulds to λ/20 by automated corrective polishing, Annals of the CIRP. 2011; 60(1): 375-378.
39. Gibson I, Rosen D, Stucker B. Additive manufacturing technologies. New York: Springer, 2010.
40. Lamikiz, A.; Sanchez, J.A.; de Lacalle, L.N.L.; Arana, J.L. Laser polishing of parts built up by selective laser sintering. Int. J. Mach. Tools Manuf. 2007, 47, 2040–2050. [CrossRef]
41. Kumstel, J.; Kirsch, B. Polishing titanium- and nickel-based alloys using cw-laser radiation. Phys. Procedia 2013, 41, 362–371. [CrossRef]
42. Steen, W.M.; Mazumder, J. Laser Material Processing; Springer: London, UK, 2010.
43. Nüsser, C.;Wehrmann, I.;Willenborg, E. Influence of intensity distribution and pulse duration on laser micro polishing. Phys. Procedia 2011, 12, 462–471. [CrossRef]
44. Alrbaey, K.; Wimpenny, D.; Tosi, R.; Manning, W.; Moroz, A. On optimization of surface roughness of selective laser melted stainless steel parts: A statistical study. J. Mater. Eng. Perform. 2014, 23, 2014–2139. [CrossRef]
45. Yasa, E.; Kruth, J. Application of laser re-melting on selective laser melting parts. Adv. Prod. Eng. Manag. 2011, 6, 259–270.
46. Rosa, B.; Mognol, P.; Hascoeth, J. Laser polishing of additive laser manufacturing surfaces. J. Laser Appl. 2015, 27, S29102. [CrossRef]

47. Rombouts, M.; Maes, G.; Hendrix,W.; Delarbre, E.; Motmans, F. Surface finish after laser material deposition. Phys. Procedia 2013, 41, 810–814. [CrossRef]
48. Marshall, G.F.; Stutz, G.E. Handbook of Optical and Laser Scanning; CRC Press: Boca Raton, FL, USA, 2011.
49. Muth, M. Optimized x/y scanning head for laser beam positioning. In Proceedings of the SPIE 2774, Design and Engineering of Optical Systems, Glasgow, UK, 23 August 1996; p. 535.
50. Yasa, E.; Kruth, J. Application of laser re-melting on selective laser melting parts. Adv. Prod. Eng. Manag. 2011, 6, 259–270.
51. Shanz, J.; Hofele, M.; Hitzler, L.; Merkel, M.; Riegel, H. Laser polishing of additive manufactured AlSi10Mg parts with an oscillating laser beam. Mach. Join. Modif. Adv. Mater. 2016, 61, 159–169.
52. Ukar, E.; Lamikiz, A.; Martinez, S.; Tabernero, I.; de Lacalle, N.L.L. Roughness prediction on laser polished surfaces. J. Mater. Process. Technol. 2012, 212, 1305–1313. [CrossRef]